nanomaterials

MDPI

Communication

Toxicity and T_2-Weighted Magnetic Resonance Imaging Potentials of Holmium Oxide Nanoparticles

Timur Sh. Atabaev [1,*], Yong Cheol Shin [2], Su-Jin Song [2], Dong-Wook Han [2,*] and Nguyen Hoa Hong [1,*]

1 Department of Physics and Astronomy, Seoul National University, Seoul 08826, Korea
2 Department of Cogno-Mechatronics Engineering, Pusan National University, Busan 46241, Korea; choel15@naver.com (Y.C.S.); songsj86@gmail.com (S.-J.S.)
* Correspondence: timuratabaev@yahoo.com (T.S.A.); nanohan@pusan.ac.kr (D.-W.H.); nguyenhong@snu.ac.kr (N.H.H.); Tel.: +82-10-3326-0512 (T.S.A.)

Received: 29 June 2017; Accepted: 2 August 2017; Published: 7 August 2017

Abstract: In recent years, paramagnetic nanoparticles (NPs) have been widely used for magnetic resonance imaging (MRI). This paper reports the fabrication and toxicity evaluation of polyethylene glycol (PEG)-functionalized holmium oxide (Ho_2O_3) NPs for potential T_2-weighted MRI applications. Various characterization techniques were used to examine the morphology, structure and chemical properties of the prepared PEG–Ho_2O_3 NPs. MRI relaxivity measurements revealed that PEG–Ho_2O_3 NPs could generate a strong negative contrast in T_2-weighted MRI. The pilot cytotoxicity experiments showed that the prepared PEG–Ho_2O_3 NPs are biocompatible at concentrations less than 16 μg/mL. Overall, the prepared PEG–Ho_2O_3 NPs have potential applications for T_2-weighted MRI imaging.

Keywords: holmium oxide; paramagnetic nanoparticles; T_2-weighted magnetic resonance imaging; toxicity

1. Introduction

Magnetic and optical metal oxide nanoparticles (NPs) have attracted considerable attention over the past three decades for biomedical imaging and diagnosis [1]. In particular, iron oxide NPs [2,3], manganese oxide NPs [4,5], and gadolinium oxide NPs [6,7] have been investigated for potential magnetic resonance imaging (MRI). However, superparamagnetic iron oxide NPs show saturation magnetization at approximately 1.5 T, which limits their MRI applicability in high magnetic fields [2]. From this point of view, paramagnetic rare-earth metal oxide NPs with higher magnetic moments and higher density of magnetic ions per surface unit are more promising for MRI applications. For example, Gd_2O_3 NPs were reported to show higher longitudinal relaxivity (r_1) compared to commercially available Gd-based chelates [8,9]. Gd_2O_3 NPs brightens the imaging place (positive contrast), because it changes the spin-lattice relaxation of water protons. On the other hand, the main limitation associated with the broad use of Gd_2O_3 NPs is in their high toxicity. In this regard, surface modification or Gd-doping into a less toxic material can be used [10,11], but these alterations can also deteriorate the relaxivity rates of the Gd_2O_3 NPs.

Other rare-earth ions, such as Dy^{3+} and Ho^{3+}, have larger magnetic moments (~10.5 μ_B) than Gd^{3+} (~8.1 μ_B). On the other hand, both Dy_2O_3 and Ho_2O_3 NPs are more suitable for T_2-weighted MRI (negative contrast) due to the fast spin relaxation of their 4*f* electrons. For example, a number of studies demonstrated the suitability of Dy_2O_3 NPs for T_2-weighted MRI [12,13]. In particular, the reported transverse r_2 relaxivities of Dy_2O_3 NPs were much higher than that of commercially available iron oxide NPs [12,13]. On the other hand, there are almost no reports of the potential toxicity and applications of Ho_2O_3 NPs as a MRI contrast nanoprobe [14]. Therefore, this study examined the

PEG-grafted Ho_2O_3 NPs to explore their toxicity and applicability as a new potential T_2-weighted MRI contrast agent. A murine fibroblast L-929 cell line was used as a pilot in-vitro model to check the cytotoxicity of the PEG–Ho_2O_3 NPs. This study suggests that the prepared PEG–Ho_2O_3 NPs can be potentially used as a new T_2-weighted MRI contrast agent at concentrations less than 16 μg/mL.

2. Materials and Methods

2.1. Synthesis Process

Analytical grade Ho_2O_3 (99.9%), HNO_3 (70%), polyethylene glycol (PEG, average M_n = 4000) and urea (99.0–100.5%) were purchased from Sigma-Aldrich (St. Louis, MO, USA) and used as received. Ho_2O_3 NPs were prepared using the reported protocols [15,16]. In brief, holmium oxide powder was converted to a holmium nitrate salt with the help of nitric acid. Later on, a sealed beaker with a freshly prepared aqueous solution of holmium nitrate (0.5 mmol in 40 mL of H_2O) was placed into a forced convection drying oven (J-300M, Jisico Co., Ltd., Seoul, South Korea) and heated to 90 °C for 1.5 h. The collected precipitates were then calcined in air at 600 °C for 1 h to produce the Ho_2O_3 NPs. PEG-functionalization of Ho_2O_3 NPs was performed according to a reported protocol [8]. The obtained colloidal solution was then dialyzed in deionized ultrapure water for 24 h to eliminate the unreacted products.

2.2. Characterization

The structure of the prepared powders was examined by X-ray diffraction (XRD, Bruker D8 Discover, Billerica, MA, USA) using Cu-Kα radiation (λ = 0.15405 nm) at a 2θ scan range 20–60°. The morphology of the particles was characterized by transmission electron microscopy (TEM, JEM-2100, JEOL Ltd., Tokyo, Japan). Energy dispersive X-ray spectroscopy (EDX, JEOL Ltd., Tokyo, Japan) was used to perform an elemental analysis. Hydrodynamic sizes and zeta potentials of the obtained nanoprobes were measured using a Nano ZS Zetasizer (Malvern Instruments Ltd., Malvern, UK). Fourier transform infrared infrared spectroscopy (FTIR, Jasco FT/IR6300, Tokyo, Japan) was used to examine the structural properties of prepared samples. The magnetization measurements were performed using a magnetic properties measurement system (MPMS-5XL/Quantum Design Inc., San Diego, CA, USA). The T_2-weighted images were obtained using a 1.5 T small animal MRI scanner (Siemens Healthinners, Enlargen, Germany). The measurement parameters used were as follows: the repetition time (TR) = 2009 ms, the time to echo (TE) = 9 ms, the field of view (FOV) = 160 × 160 mm, slice thickness = 5 mm, matrix = 256 × 256, number of excitations (NEX) = 1. All characterization measurements were performed at a room temperature of 22 ± 1 °C. The conditions for cell culture, cytotoxicity assay, fluorescence assay and statistical analysis were reported in our previous report [11].

3. Results and Discussion

Paramagnetic NPs for multimodal imaging have attracted considerable interest in recent years for potential nanomedical applications. Ultrasmall holmium oxide Ho_2O_3 NPs were proposed recently for potential MRI imaging applications [14]. However, the biocompatibility of Ho_2O_3 NPs is still a big issue to be addressed. Furthermore, it is very important to develop eco-friendly and low-cost synthesis method for fabricating the highly monodispersed Ho_2O_3 NPs at large scales. To address these issues, we designed a simple two-step approach to synthesize the highly monodispersed PEG–Ho_2O_3 NPs. The successful synthesis of PEG–Ho_2O_3 NPs is confirmed with several analysis techniques. XRD was used to examine the structural properties of the as-prepared Ho_2O_3 NPs. Figure 1a shows an XRD pattern of the as-prepared Ho_2O_3 NPs. The XRD peaks were assigned to the standard cubic (Ia_3) Ho_2O_3 structure (JCPDS no. 43-1018) [17]. No additional impurity peaks were detected; thus, the obtained nanoprobes can be considered a pure cubic Ho_2O_3 phase. Energy dispersive X-ray spectroscopy (Figure 1b) revealed the presence of Ho and O elements only, indicating the formation of a pure Ho_2O_3 structure after a calcination process.

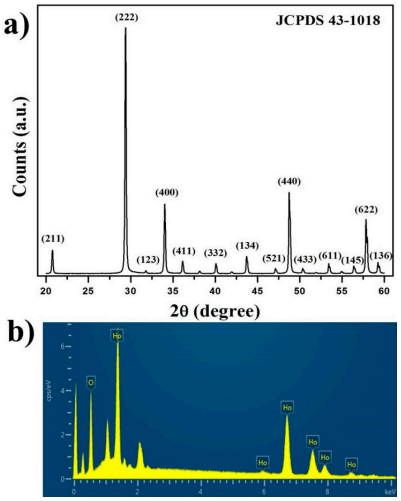

Figure 1. (**a**) X-ray diffraction (XRD) and (**b**) EDX analysis of as-prepared Ho_2O_3 nanoparticles (NPs).

Figure 2 presents the morphology and size distribution of the as-prepared PEG–Ho_2O_3 NPs. According to transmission electron microscopy, the prepared nanoprobes had an almost spherical morphology within the range 67–81 nm. On the other hand, the measured hydrodynamic sizes of PEG–Ho_2O_3 NPs were in the range of 80–90 nm (polydispersity index PDI = 1.67). The difference between observed and measured sizes can be explained by hydration coverage and existence of a thin PEG layer on the Ho_2O_3 NPs surface [18]. FTIR analysis (Figure 3) was used to examine the successful PEG-functionalization on the surface of Ho_2O_3 NPs. The PEG–Ho_2O_3 NPs showed the angular deformation of water molecules (~1660 cm^{-1}) and the stretching vibrations of the OH group (~3600 cm^{-1}). In addition, FTIR analysis showed the scissoring (~1470 cm^{-1}) and waging (~1340 cm^{-1}) modes of the CH_2 group of the PEG chain. A most prominent peak at ~1100 cm^{-1} was also assigned to the PEG chain C–O–C vibration [8]. Thus, FTIR analysis confirmed the presence of water and PEG molecules on the surface of Ho_2O_3 NPs. A thin PEG layer on the Ho_2O_3 NPs surface can enhance the steric repulsion and prolong the blood circulation time [8]. In addition, one can achieve higher biocompatibility of prepared NPs through the PEG surface functionalization. The zeta potential was further measured at the physiological pH of 7.4 to ensure the colloidal stability of the PEG–Ho_2O_3 NPs. The measured zeta potential for PEG–Ho_2O_3 NPs was approximately (−16.7 mV). Therefore, the colloidal solution of PEG–Ho_2O_3 NPs can be stable for a relatively long time.

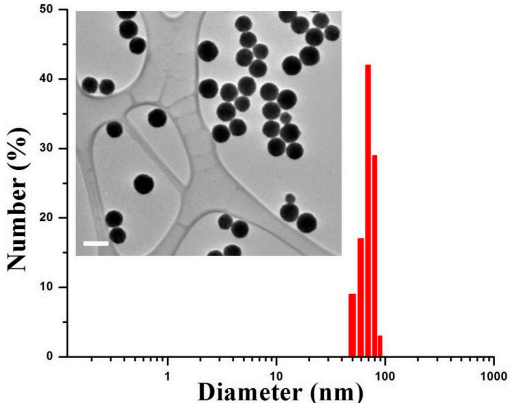

Figure 2. Measured hydrodynamic sizes of polyethylene glycol functionalized holmium oxide (PEG–Ho_2O_3) NPs. Inset is a transmission electron microscopy (TEM) image of PEG–Ho_2O_3 NPs (bar scale = 100 nm).

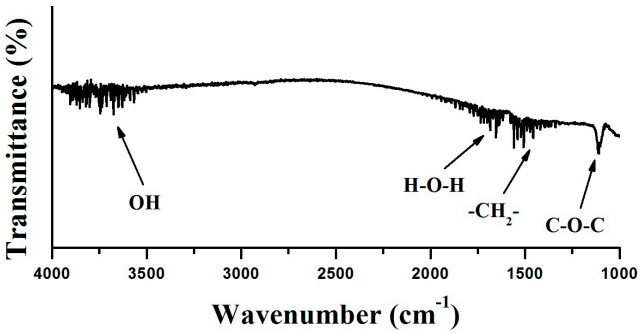

Figure 3. Fourier transform infrared spectroscopy (FTIR) analysis of PEG–Ho_2O_3 NPs.

The magnetic properties of prepared PEG–Ho_2O_3 NPs were investigated further using an MPMS. Figure 4a shows the M(H) curve for the prepared PEG–Ho_2O_3 NPs at room temperature (T = 300 K). The observed linear relationship between the magnetization and applied field shows typical paramagnetic behavior of PEG–Ho_2O_3 NPs at room temperature. Figure 4b shows the measured inverse $1/T_2$ relaxation times vs. Ho^{3+} concentration. The transverse r_2 relaxivity rate was estimated from a linear fit of $1/T_2$ vs. Ho^{3+} concentration. The slope of the linear fit revealed a transverse relaxation rate (r_2) of 23.47 $mM^{-1}{\cdot}s^{-1}$. One can also easily observe that the r_2 map images become darker with increasing Ho^{3+} concentration (Figure 4b, Inset). The obtained r_2 value of PEG–Ho_2O_3 NPs is much higher than the reported transverse relaxation rate (r_2 = 17.95 $mM^{-1}{\cdot}s^{-1}$) for Mn-doped iron oxide NPs [19]. It should be also noted that magnetic moment of Ho_2O_3 is not saturated at room temperature compared to widely employed iron oxide NPs [14]. As a result, the magnetic moment of PEG–Ho_2O_3 NPs will further increase with an increase in the applied magnetic fields. Therefore, the prepared PEG–Ho_2O_3 NPs can be applied as a T_2-weighted MRI agent, particularly at high magnetic fields, because their contrast enhancements will increase with an increase magnetic field [12,13].

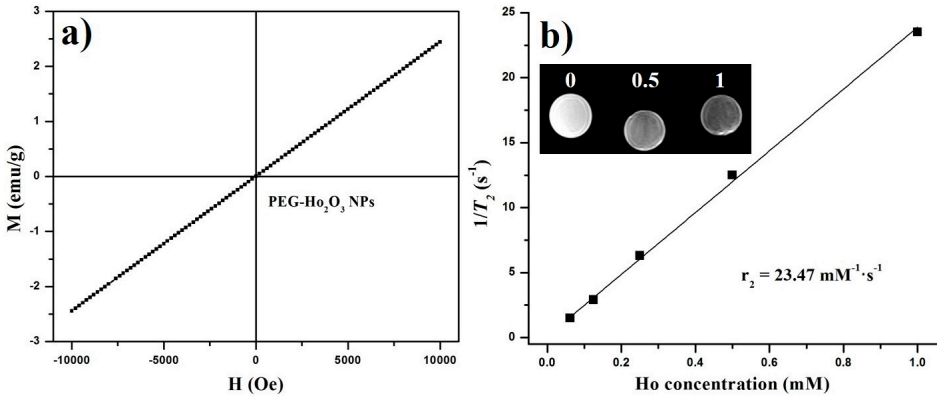

Figure 4. (**a**) Measured M(H) curve at 300 K; (**b**) r_2 relaxation rate ($1/T_2$) vs. Ho^{3+} concentration (mM). Inset is r_2 map images of PEG–Ho_2O_3 NPs aqueous solution at different concentrations.

The toxicity of the prepared NPs is another important factor that should be taken into consideration for potential nanomedical applications. Figure 5 presents the cytotoxicity profiles of the PEG–Ho_2O_3 NPs in L-929 fibroblastic cells using a WST-8 assay [10,11]. Metal ions can generate reactive oxygen species in the cell interior ("Trojan horse" mechanism), which leads to oxidative stress to living cells [20]. Therefore, the cytotoxicity results showed an obvious dose-dependent decrease in their relative cell viability. Obviously, PEG–Ho_2O_3 NPs caused no significant decrease in cell viability up to 16 μg/mL. Considering the in-vitro cytotoxicity only, the PEG–Ho_2O_3 NPs can be used at

concentrations less than 16 μg/mL. However, the cytotoxicity against the cells exposed to PEG–Ho_2O_3 NPs must be tested by other viability end-point measurements.

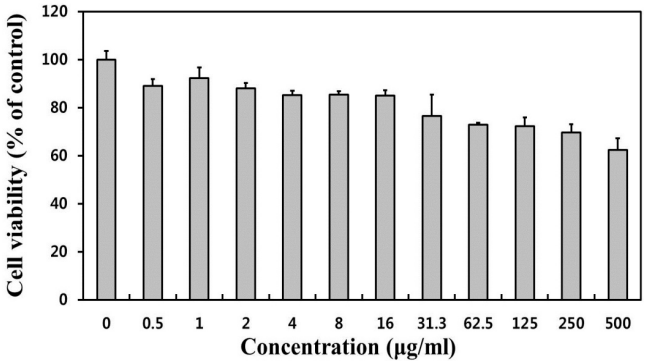

Figure 5. Cytotoxicity profiles of PEG–Ho_2O_3 NPs in L-929 fibroblastic cells.

Fluorescence microscopy (IX81-F72, Olympus Optical, Osaka, Japan) was used to visualize the cellular uptake and distribution of PEG–Ho_2O_3 NPs within the cultured L-929 cells. Figure 6a shows the phase contrast image of L-929 cells after incubation with PEG–Ho_2O_3 NPs suspension (10 μg/mL). The phase contrast image showed that the L-929 cells labeled with PEG–Ho_2O_3 NPs spread well with normal fibroblast-like morphologies. Although a detailed study for the cellular uptake was not performed, it is believed that the PEG–Ho_2O_3 NPs permeated into the cell membrane by non-specific endocytosis rather than pinocytosis [10,20]. Figure 6b shows that the prepared PEG–Ho_2O_3 NPs can also emit green light due to the intra 4*f*-transitions in holmium ions [21]. Therefore, prepared PEG–Ho_2O_3 NPs can be simultaneously utilized as a bimodal nanoprobe for MRI and optical imaging.

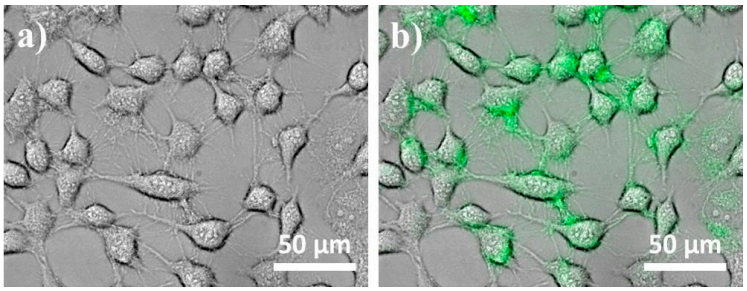

Figure 6. Phase contrast (**a**) and fluorescence (**b**) images of L-929 fibroblastic cells incubated with 10 μg/mL of PEG–Ho_2O_3 NPs.

4. Conclusions

In summary, PEG–Ho_2O_3 NPs were prepared and their applicability as new T_2-weighted MRI contrast nanoprobes was assessed. Cytotoxicity measurements showed that the prepared PEG–Ho_2O_3 NPs were nontoxic at concentrations less than 16 μg/mL. MRI relaxivity studies revealed high transverse relaxivity (r_2 = 23.47 $mM^{-1}{\cdot}s^{-1}$), suggesting that the prepared PEG–Ho_2O_3 NPs can be used as an efficient T_2-weighted nanoprobe. In addition, green fluorescence was also detected from the PEG–Ho_2O_3 NPs due to intra 4*f*-transitions in holmium ions. Therefore, the prepared PEG–Ho_2O_3 NPs could be used as a dual-imaging nanoprobe.

Acknowledgments: This work was supported by the BK21 PLUS program at the Department of Physics and Astronomy, Seoul National University. This research was financially supported by Basic Science Research Program through the National Research Foundation of Korea (NRF) funded by the Ministry of Education

(No. 2016R1D1A1B03931076). Part of this study has been performed using facilities at IBS Center for Correlated Electron Systems, Seoul National University.

Author Contributions: Timur Sh. Atabaev and Nguyen Hoa Hong conceived and designed the experiments; Timur Sh. Atabaev performed the synthesis and characterization of the samples; Yong Cheol Shin and Su-Jin Song performed the cytotoxicity and cellular imaging experiments; Timur Sh. Atabaev, Dong-Wook Han and Nguyen Hoa Hong analyzed the data; Timur Sh. Atabaev wrote the paper.

Conflicts of Interest: The authors declare no conflict of interest.

References

1. Atabaev, T.S.; Kim, H.K.; Hwang, Y.H. Fabrication of bifuctional core-shell Fe_3O_4 particles coated with ultrathin phosphor layer. *Nanoscale Res. Lett.* **2013**, *8*, 357. [CrossRef] [PubMed]
2. Gautam, A.; van Veggel, F.C.J.M. Synthesis of nanoparticles, their biocompatibility, and toxicity behavior for biomedical applications. *J. Mater. Chem. B* **2013**, *1*, 5186–5200. [CrossRef]
3. Sun, C.; Sze, R.; Zhang, M. Folic acid-PEG conjugated superparamagnetic nanoparticles for targeted cellular uptake and detection by MRI. *J. Biomed. Mater. Res. A* **2006**, *78A*, 550–557. [CrossRef] [PubMed]
4. Ding, X.; Liu, J.; Li, J.; Wang, F.; Wang, Y.; Song, S.; Zhang, H. Polydopamine coated manganese oxide nanoparticles with ultrahigh relaxivity as nanotheranostic agents for magnetic resonance imaging guided synergetic chemo-/photothermal therapy. *Chem. Sci.* **2016**, *7*, 6695–6700. [CrossRef] [PubMed]
5. Shin, J.; Anisur, R.M.; Ko, M.K.; Im, G.H.; Lee, J.H.; Lee, I.S. Hollow manganese oxide nanoparticles as multifunctional agents for magnetic resonance imaging and drug delivery. *Angew. Chem. Int. Ed. Engl.* **2009**, *48*, 321–324. [CrossRef] [PubMed]
6. Atabaev, T.S.; Lee, J.H.; Han, D.W.; Kim, H.K.; Hwang, Y.H. Fabrication of carbon coated gadolinia particles for dual-mode magnetic resonance and fluorescence imaging. *J. Adv. Ceram.* **2015**, *4*, 118–122. [CrossRef]
7. Faucher, L.; Gossuin, Y.; Hocq, A.; Fortin, M.A. Impact of agglomeration on the relaxometric properties of paramagnetic ultra-small gadolinium oxide nanoparticles. *Nanotechnology* **2011**, *22*, 295103. [CrossRef] [PubMed]
8. Atabaev, T.S.; Lee, J.H.; Han, D.W.; Kim, H.K.; Hwang, Y.H. Ultrafine PEG-capped gadolinia nanoparticles: Cytotoxicity and potential biomedical applications for MRI and luminescent imaging. *RSC Adv.* **2014**, *4*, 34343–34349. [CrossRef]
9. Chen, F.; Chen, M.; Yang, C.; Liu, J.; Luo, N.; Yang, G.; Chen, D.; Li, L. Terbium-doped gadolinium oxide nanoparticles prepared by laser ablation in liquid for use as a fluorescence and magnetic resonance imaging dual-modal contrast agent. *Phys. Chem. Chem. Phys.* **2015**, *17*, 1189–1196. [CrossRef] [PubMed]
10. Atabaev, T.S.; Lee, J.H.; Han, D.W.; Choo, K.S.; Jeon, U.B.; Hwang, J.Y.; Yeom, J.A.; Kang, C.; Kim, H.K.; Hwang, Y.H. Multicolor nanoprobes based on silica-coated gadolinium oxide nanoparticles with highly reduced toxicity. *RSC Adv.* **2016**, *6*, 19758–19762. [CrossRef]
11. Atabaev, T.S.; Lee, J.H.; Shin, Y.C.; Han, D.W.; Choo, K.S.; Jeon, U.B.; Hwang, J.Y.; Yeom, J.A.; Kim, H.K.; Hwang, Y.H. Eu, Gd-codoped yttria nanoprobes for optical and T_1-weighted magnetic resonance imaging. *Nanomaterials* **2017**, *7*, 35. [CrossRef] [PubMed]
12. Norek, M.; Kampert, E.; Zeitler, U.; Peters, J.A. Tuning of the size of Dy_2O_3 nanoparticles for optimal performance as an MRI contrast agent. *J. Am. Chem. Soc.* **2008**, *130*, 5335–5340. [CrossRef] [PubMed]
13. Norek, M.; Pereira, G.A.; Geraldes, C.F.G.C.; Denkova, A.; Zhou, W.; Peters, J.A. NMR transversal relaxivity of suspensions of lanthanide oxide nanoparticles. *J. Phys. Chem. C* **2007**, *111*, 10240–10246. [CrossRef]
14. Kattel, K.; Kim, C.R.; Xu, W.; Kim, T.J.; Park, J.W.; Chang, Y.; Lee, G.H. Synthesis, magnetic properties, map images, and water proton relaxivities of D-glucuronic acid coated Ln_2O_3 nanoparticles (Ln = Ho and Er). *J. Nanosci. Nanotechnol.* **2015**, *15*, 7311–7316. [CrossRef] [PubMed]
15. Atabaev, T.S.; Vu, H.H.T.; Kim, H.K.; Hwang, Y.H. The optical properties of Eu^{3+} and Tm^{3+} co-doped Y_2O_3 submicron particles. *J. Alloys Compd.* **2012**, *525*, 8–13. [CrossRef]
16. Atabaev, T.S.; Vu, H.H.T.; Kim, H.K.; Hwang, Y.H. Ratiometric pH sensor based on fluorescent core-shell nanoparticles. *J. Nanosci. Nanotechnol.* **2017**, *17*, 8313–8316.
17. Pandey, S.D.; Samanta, K.; Singh, J.; Sharma, N.D.; Bandyopadhyay, A.K. Raman scattering of rare earth sesquioxide Ho_2O_3: A pressure and temperature dependent study. *J. Appl. Phys.* **2014**, *116*, 133504. [CrossRef]

18. Faucher, L.; Tremblay, M.; Lagueux, J.; Gossuin, Y.; Fortin, M.A. Rapid synthesis of PEGylated ultrasmall gadolinium oxide nanoparticles for cell labeling and tracking with MRI. *ACS Appl. Mater. Interfaces* **2012**, *4*, 4506–4515. [CrossRef] [PubMed]
19. Zhang, M.; Cao, Y.; Wang, L.; Ma, Y.; Tu, X.; Zhang, Z. Manganese doped iron oxide theranostic nanoparticles for combined T_1 magnetic resonance imaging and photothermal therapy. *ACS Appl. Mater. Interfaces* **2015**, *7*, 4650–4658. [CrossRef] [PubMed]
20. Atabaev, T.S.; Lee, J.H.; Han, D.W.; Hwang, Y.H.; Kim, H.K. Cytotoxicity and cell imaging potentials of submicron color-tunable yttria particles. *J. Biomed. Mater. Res. A* **2012**, *100A*, 2287–2294. [CrossRef] [PubMed]
21. Atabaev, T.S.; Vu, H.H.T.; Kim, Y.D.; Lee, J.H.; Kim, H.K.; Hwang, Y.H. Synthesis and luminescence properties of Ho^{3+} doped Y_2O_3 submicron particles. *J. Phys. Chem. Solids* **2012**, *73*, 176–181. [CrossRef]